

Review

Progress in the Development of Active-Matrix Quantum-Dot Light-Emitting Diodes Driven by Non-Si Thin-Film Transistors

Geun Woo Baek ¹, Yeon Jun Kim ¹, Minhyung Lee ¹, Yeunwoo Kwon ¹, Beomsoo Chun ¹, Ganghyun Park ¹, Hansol Seo ¹, Heesun Yang ^{2,*} and Jeonghun Kwak ^{1,*}

¹ Department of Electrical and Computer Engineering, Inter-University Semiconductor Research Center, Soft Foundry Institute, Seoul National University, Seoul 08826, Republic of Korea

² Department of Materials Science and Engineering, Hongik University, Seoul 04066, Republic of Korea

* Correspondence: hyang@hongik.ac.kr (H.Y.); jkwak@snu.ac.kr (J.K.)

Abstract: This paper aims to discuss the key accomplishments and further prospects of active-matrix (AM) quantum-dot (QD) light-emitting diodes (QLEDs) display. We present an overview and state-of-the-art of QLEDs as a frontplane and non-Si-based thin-film transistors (TFTs) as a backplane to meet the requirements for the next-generation displays, such as flexibility, transparency, low power consumption, fast response, high efficiency, and operational reliability. After a brief introduction, we first review the research on non-Si-based TFTs using metal oxides, transition metal dichalcogenides, and semiconducting carbon nanotubes as the driving unit of display devices. Next, QLED technologies are analyzed in terms of the device structure, device engineering, and QD patterning technique to realize high-performance, full-color AM-QLEDs. Lastly, recent research on the monolithic integration of TFT-QLED is examined, which proposes a new perspective on the integrated device. We anticipate that this review will help the readership understand the fundamentals, current state, and issues on TFTs and QLEDs for future AM-QLED displays.



Citation: Baek, G.W.; Kim, Y.J.; Lee, M.; Kwon, Y.; Chun, B.; Park, G.; Seo, H.; Yang, H.; Kwak, J. Progress in the Development of Active-Matrix Quantum-Dot Light-Emitting Diodes Driven by Non-Si Thin-Film Transistors. *Materials* **2022**, *15*, 8511. <https://doi.org/10.3390/ma15238511>

Academic Editor: Stefano Agnoli

Received: 19 October 2022

Accepted: 27 November 2022

Published: 29 November 2022

Publisher's Note: MDPI stays neutral with regard to jurisdictional claims in published maps and institutional affiliations.



Copyright: © 2022 by the authors. Licensee MDPI, Basel, Switzerland. This article is an open access article distributed under the terms and conditions of the Creative Commons Attribution (CC BY) license (<https://creativecommons.org/licenses/by/4.0/>).

Keywords: active-matrix; quantum-dot light-emitting diodes; thin film transistors; metal oxides; transition metal dichalcogenides; carbon nanotubes

1. Introduction

Colloidal quantum dots (QDs) have been regarded as promising emitters owing to their excellent optical properties, such as near-unity photoluminescence (PL) quantum yield (QY), narrow emission spectral bandwidth, and size-dependent bandgap tunability. Based on these merits, QDs can be utilized for a variety of applications, such as display devices, solar cells, and photodetectors [1–10]. In particular, QDs have been widely investigated for their use in display devices to improve the color gamut. For instance, a liquid crystal display (LCD), including a QD-based color conversion film, has already been commercialized. Meanwhile, interest in QD-based light-emitting diodes (QLEDs) has been increasing for decades to take advantage of their superb optoelectronic performance, solution-processability, and fabrication compatibility with existing technologies, which enabled QLEDs to exhibit high efficiency, luminance, and stability comparable with those of organic light-emitting diodes (OLEDs) [11–16]. Additionally, the demonstration of active-matrix (AM) QLED displays using a Si-based thin-film transistors (TFTs) backplane has been raising the expectation for high-quality displays [17–22]. Despite the remarkable development, however, further research on AM-QLEDs driven by non-Si-based TFTs is required to realize display devices with advanced features, e.g., transparency, flexibility, and stretchability, which has rarely been reported so far [23–26]. This may be because the TFT backplane needs to meet more stringent requirements, such as good electrical properties to drive high current, low response to light from QLED, and endurance to the solution-based QLED fabrication processes [27–31].

increase the resistance causing Joule heating, which thus can reduce the response speed and degrade the reliability of the TFT backplane. Therefore, the development of p-type TFTs is necessary for high-performance AM-QLEDs. Previously, oxides were also one of the p-type channel candidates. However, p-type oxides, such as NiO, SnO, and CuO, mostly suffer from the lack of stability and possess an anisotropic, localized O 2p orbital with a large hole effective mass, leading to μ_h of $<1 \text{ cm}^2 \text{ V}^{-1} \text{ s}^{-1}$ [44–47].

As an alternative, TMDCs in a chemical composition of MX_2 , where M is a transition metal (Mo, W, etc.) and X is a chalcogen (S, Se, or Te), have been focused as a promising p-channel material owing to their advanced properties, such as tunable bandgap depending on the number of layers, absence of dangling bonds, and resultingly a high on–off ratio with decent mobility. In addition, it is possible to form a functional heterostructure of two different materials. Among various TMDCs, MoTe_2 can be a good choice for a TFT backplane because of its a few distinctive characteristics, i.e., insensitivity to light, easy type-convertibility, and bias stress instability [23,25,48]. On the other hand, exfoliation-based deposition and fine-patterning of the TMDC monolayer are the major obstacles to their application in large-area AM displays. Although technologies for high-resolution and large-scale fabrication have consistently progressed [49–51], they need to be developed more to satisfy customer expectations for large-sized displays.

For the large-area processability, semiconducting SWNTs would be an option for the TFT channel. The SWNT-based TFTs are easily fabricated using various solution processes at low temperatures, and they also show high device performance with intrinsic field-effect mobility (μ_h of up to $\sim 10^2 \text{ cm}^2 \text{ V}^{-1} \text{ s}^{-1}$), flexibility, and transparency [52–55]. They are also resistant to the subsequent processes for patterning and QLED deposition. Contrary to the advantages, there are a few known issues of SWNTs, such as low chirality and poor dispersity in solution—though the chirality is improving gradually, reaching 99.999% or even higher purity through post-treatment [56–58], and the dispersity has been enhanced by wrapping with DNA or conjugated polymers [59–62]. Poor n-type performance of SWNTs also needs to be enhanced for practical use in a display backplane, to be combined with an inverted QLED. A few of the TFT performances using oxides, TMDCs, and SWNTs reported within five years are summarized in Table 1.

Organic semiconductors have also been considered as active channel materials. Several small molecules (e.g., pentacene, thienothiophene derivatives) and polymers have been studied owing to their low cost and facile fabrication with high scalability [63–65]. However, it has limitations to employ as backplane TFTs due to its low mobility, high threshold voltage, low BTS, and patterning issues [66,67]. These problems need to be overcome for their practical use in backplanes.

Table 1. Summary of TFT parameters using oxides, TMDCs, and SWNTs.

Year	Channel Material	Type	Mobility ($\text{cm}^2 \text{ V}^{-1} \text{ s}^{-1}$)	Subthreshold Swing (V dec^{-1})	$I_{\text{on/off}}$ Ratio	Threshold Voltage (V)	Reference
2018	IGZO	n	61.3	0.08	$\sim 10^6$	0.78	[68]
	MoS_2	n	260	-	$\sim 10^6$	-	[69]
	SWNT	n	10	-	$\sim 10^8$	-	[70]
2019	IGZO	n	74	0.21	$\sim 10^8$	-1.3	[41]
	MoS_2	n	170	-	$\sim 10^6$	-	[71]
	SWNT	p	20.9	0.2	$\sim 10^4$	0.4	[72]
2020	ZnON	n	147	0.21	$\sim 10^4$	-0.72	[40]
	MoS_2	n	107	-	$\sim 10^6$	-	[73]
	SWNT	p	16	-	-	-	[74]
	MoTe_2	p	178.7	-	$\sim 10^7$	-22	[75]

Table 1. Cont.

Year	Channel Material	Type	Mobility ($\text{cm}^2 \text{V}^{-1} \text{s}^{-1}$)	Subthreshold Swing (V dec^{-1})	$I_{\text{on/off}}$ Ratio	Threshold Voltage (V)	Reference
2021	IGTO *	n	116.5	0.13	$\sim 10^9$	0.47	[76]
	MoS ₂	n	44.6	0.36	$\sim 10^5$	-	[77]
	SWNT	p	10.92	0.4	$\sim 10^5$	0.48	[78]
	MoTe ₂	p	12.6	0.26	$\sim 10^4$	0.87	[79]
2022	In ₂ O ₃ :H	n	139.2	0.19	-	0.2	[43]
	MoS ₂	n	12.3	-	$\sim 10^9$	-	[80]
	SWNT	p	496	-	$\sim 10^8$	-	[81]
	MoTe ₂	p	30	-	$\sim 10^6$	-20	[82]

* Indium-Gallium-Tin-Oxide.

3. QLED Frontplane Technology

A QLED is a device for utilizing electroluminescence (EL) from QDs, consisting of hole injection/transport layers (HIL/HTL), electron injection/transport layers (EIL/ETL), and a QD emissive layer between them, similar to an OLED structure. Since the first QLED was reported [83], the efficiency and operational lifetime have been improved owing to the advances in QD synthesis, surface treatment, device architecture, and fundamental understandings of the QLEDs [84]. To realize the AM-QLED display, QLEDs should have high efficiency and brightness for low power consumption and a long operational lifetime for maintaining image quality. High-resolution patterning of the QD layer is also required for future display devices. Improvement of electron–hole balance in a QLED is the most significant issue to be solved because it is directly related to several kinds of non-radiative recombination processes (e.g., Auger recombination and exciton–polaron quenching) which affect the QLED efficiency and efficiency roll-off. Despite multilateral efforts, it is not easy to fundamentally overcome this issue due to a few inherent characteristics of QDs and QLEDs—an extremely narrow exciton recombination zone [85] and large energy level offsets with poor interfacial morphology at the QD–organic interface. According to the device structure and process compatibility, the integration of a QLED with a driving TFT needs to be studied. In this section, we briefly review the progress of QLEDs toward high-performance AM-QLEDs from the viewpoints of the device structure and engineering of the QDs and charge transport layers for improved electron–hole balance.

3.1. Device Architecture for QLEDs

The device architecture of QLEDs can be classified in a number of ways. According to the stacking order of each functional layer, QLEDs can be distinguished into two types, a normal structure (also called a conventional or standard structure) and an inverted structure. Figure 3a shows a normal QLED structure with a schematic energy band diagram, which is composed in a sequence of the anode, HIL, HTL, QDs, ETL, EIL, and cathode from the substrate. Because solution-based QD deposition is likely to damage the underlying organic HIL/HTL layers, the selectivity of charge-transporting materials and fabrication steps are significantly influenced in this structure. Also, an HTL possessing a deep, highest-occupied-molecular-orbital (HOMO) energy level is favorable for hole injection from organic HTL to inorganic QDs due to a large energy barrier between them. On the contrary, an inverted QLED is produced in the opposite order, from the cathode at the bottom to the anode on the top, as depicted in Figure 3b. As reported previously [86], this structure is beneficial for electron injection from the bottom cathode to QDs by adopting metal oxide nanoparticles (e.g., ZnO, ZnMgO, SnO, etc.) as the ETL with resistance to the follow-up QD deposition process. They have a good μ_e of approximately 10^{-4} – $10^{-3} \text{ cm}^2 \text{V}^{-1} \text{s}^{-1}$ and well-alignment of the conduction band level with QDs [86]. The relatively high charge density of metal oxides can transfer electrons to negatively charge QDs even without bias, facilitating electron injection into QDs by Auger-assisted carrier injection [87,88]. It also allows the expanded

choice of HTL materials with the desired energy levels and mobility for boosting the hole injection using various deposition methods. Lastly, the stacking order has an influence on QLED–TFT integration. Considering that QLED fabrication starts on a substrate with a TFT array, it is more propitious to combine a normal QLED with a p-type TFT to supply hole current to the bottom anode or, similarly, an inverted QLED with an n-type TFT.

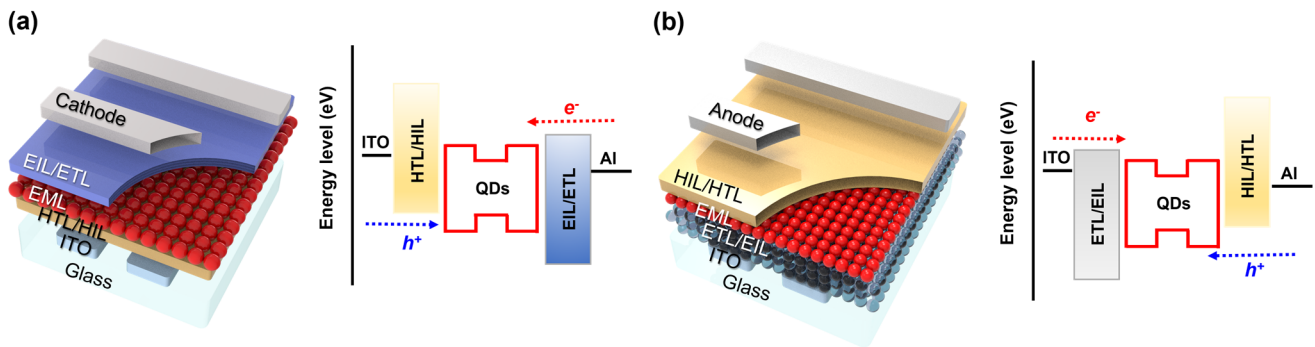


Figure 3. QLED device architecture with a schematic energy band diagram: (a) A normal structure and (b) an inverted structure.

Depending on the direction of light emission, QLEDs are divided into bottom- and top-emission structures, which should be taken into consideration when designing the AM-QLEDs. In the case of the bottom-emission structure, the AM-QLED backplane must be transparent because the light emitted from the QLED subpixel needs to travel through the substrate. But as opaque metal wiring and TFTs below QLEDs reduce the aperture ratio, the bottom-emission structure is limitedly used for large-area displays. On the other hand, the top-emission structure, consisting of a completely reflective bottom electrode and a (semi-)transparent top electrode, emits light in the opposite direction of the substrate. Thus, it guarantees light emission from the full-subpixel area without any impediments, leading to being commonly applied for small-sized displays. No substrate in the optical path may considerably improve the light outcoupling efficiency [89–91]. Also, a microcavity effect between two metallic electrodes can be utilized to tune the peak wavelength and enhance the color purity [92–95]. However, intense light emission in the normal direction results in a distorted angular profile of the Lambertian distribution, which may cause a poor viewing angle in display devices. Recently, a highly efficient top-emitting QLED with an angular-independent emission profile was demonstrated by introducing a nanosphere scattering layer [96]. Also, a high external quantum efficiency (EQE) of 32.5% was achieved by enhancing the light extraction efficiency owing to the reduced absorption and waveguide losses and minimizing the surface plasmon polariton mode at the metal–dielectric interface. More studies on top-emitting QLEDs are needed, considering the significance of this topic to the industry.

A tandem structure, composed of two or more EL units connected in series, is also applicable to QLEDs. Since a QLED is driven by current, an electrical series connection of them enables the operation of all the EL stacks at the same current level. Thus, the EQE and current efficiency tend to increase roughly in proportion to the number of EL units, but the driving voltage increases so that the power efficiency remains the same or slightly lower due to increased internal resistance [97–100]. Between each EL unit, a charge generation layer (CGL) or an interconnecting layer should be formed, in which electrons and holes are generated and supplied to adjacent two units, respectively. For that, the CGL generally comprises a planar heterojunction (e.g., p–n junction or p–metal junction) for efficient charge separation with properties of low resistance and high transparency. Particularly in QLEDs, the CGL deposition process needs to be compatible with the fabrication process of each EL unit, which makes it hard to stack multiple QLED units.

3.2. High-Performance QLEDs Based on Device Engineering

Within a certain QLED structure, we can further modify the properties of each constituting layer to improve device performance. In particular, poor charge balance is one critical issue in this research field, which can be resolved mainly by device engineering. For this, various approaches and methods have been suggested, such as doping or blending a charge transporting layer (CTL) or insertion of an additional layer, and QD surface treatment. First, changing the properties of the CTL by doping or mixing an additional material is an intuitive method. As mentioned above, there have been difficulties in hole injection into QDs, leading to a large number of researches on HTL modification. Doping the HTL with an electron acceptor, e.g., 2,3,5,6-tetrafluoro-7,7,8,8-tetracyanoquinodimethane (F4-TCNQ) and MoO_x, improves hole conduction ability and further enhances the thermal stability of the HTL [101,102]. A composite HTL serves complementary properties of two materials in terms of energy level, mobility, and morphology, as shown in Figure 4a. In detail, small molecule–polymer composites typically exhibit good mobility from a small molecule in a robust polymer matrix. Representative small molecules for this purpose are 4,4'-bis(N-(3-methylphenyl)-N-phenylamino)biphenyl (TPD), 4,4',4'-tris(carbazol-9-yl)triphenylamine (TCTA) and 4,4',N,N'-diphenylcarbazole (CBP), and widely-used matrix polymers are poly[N,N'-bis(4-butylphenyl)-N,N'-bis(phenyl)-benzidine] (poly-TPD), poly(9,9-dioctylfluorene-*alt*-N-(4-*sec*-butylphenyl)-diphenylamine) (TFB), and poly-N-vinyl carbazole (PVK) [103–111].

The properties of the ETL can also be modified by doping and additives. For instance, ZnO has good electrical properties for QLEDs but has defect states from intrinsic oxygen vacancy, resulting in device instability and severe exciton quenching. Metal-doped/alloyed ZnO, such as ZnMgO and Li/Al/Ga-doped ZnO, has been reported to show improved device performance of QLEDs [112–115]. Inserting an additional layer has also been demonstrated for high-performance QLEDs. Especially, the insertion of a poly(methylmethacrylate) (PMMA) layer near the QD layer effectively blocks leakage current through the QD layer to obtain high EQE [116,117]. Similar effects were reported by incorporating a thin insulating layer (e.g., Al₂O₃, polyethylenimine ethoxylated) and a thin semiconducting organic layer having low mobility and wide bandgap [118–121].

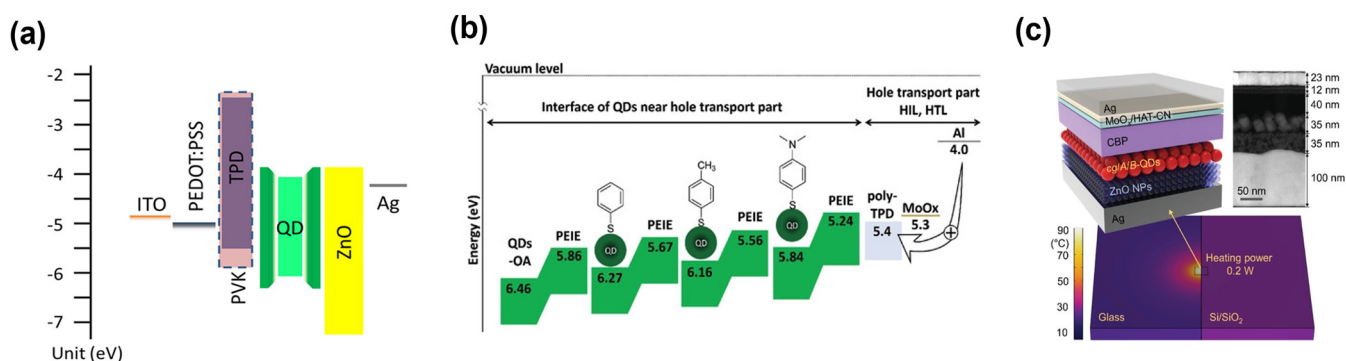


Figure 4. Device engineering methods: (a) Composite of PVK and TPD as the HTL for the QLED (Reproduced from [105] with permission from American Chemical Society). (b) Energy band diagram of the green QLED with interface-modified QDs (Reproduced from [122] with permission from Wiley). (c) Schematic illustration of an inverted top-emission QLED fabricated on substrates with a different heat dissipation property (Reproduced from [123] with permission from Wiley).

Modification of the QD surface with proper ligands is also an important strategy for achieving high performance because insulating surfactants surrounding the QDs can hinder charge transport. A few methods have been reported to improve the optoelectronic properties by QD surface modification, such as ligand exchange with shorter ligands, electron donating/accepting ligands, and semiconducting ligands. Ligands with shorter alkyl chains or smaller molecules instead of oleic acids may provide dense, uni-

form, and stable packing of QDs, resulting in enhanced carrier injection/transport in QLEDs [122,124–127]. Adopting the ligand with a strong dipole moment originating from the electron donor/acceptor group can shift the energy level of QDs, which is helpful for balancing charge injection into QDs. For example, 2-ethylhexane-1-thiol ligands upshifted the energy level of $\text{Zn}_{1-x}\text{Cd}_x\text{Se}/\text{ZnSe}/\text{ZnS}$ QDs and reduced the hole injection barrier, resulting in a current efficiency of 72 cd A^{-1} , the maximum luminance of $334,000 \text{ cd m}^{-2}$, and a half-lifetime of 140 h at an initial luminance (L_0) of $17,200 \text{ cd m}^{-2}$ which corresponds to that of 1,800,000 h at L_0 of 100 cd m^{-2} by estimation [8].

Also, precise tuning of the energy level of QDs was demonstrated by ligand exchange with the series of thiophenol derivatives having a negative dipole moment, as shown in Figure 4b [122]. As a result, a green QLED exhibited improved current efficiency and maximum luminance of 98.2 cd A^{-1} and $106,400 \text{ cd m}^{-2}$, respectively. Furthermore, QD surface treatment with halide anions can be a promising approach to enhance the QLED performance [14,113,125]. Ligand exchange and treatment with halides have effects in improving charge transport properties and reducing defects of QDs. Instead of insulating ligands, semiconducting ligands, which have a good charge transport property, have also been of interest for charge balance in QLEDs [126,127]. For the semiconducting property, the ligands typically contain bulkier functional groups in the form of oligomers or polymers. Thus, the QD film shows increased dot-to-dot distance but improved charge transport ability. Furthermore, it leads to the widening of the exciton recombination zone in the thicker emitting layer, which is ideal for reducing the efficiency roll-off.

Upon engineering the internal device structure, the introduction of a new substrate having a high thermal conductivity has recently been of interest in reducing thermal degradation. Joule heating is unavoidable in current-driven QLEDs, which deteriorates the efficiency and stability of the devices. Low thermal conductivity of the widely-used glass substrate ($\sim 1.0 \text{ W m}^{-1} \text{ K}^{-1}$) hinders heat dissipation and thereby increases the temperature of subpixels, which is known to accelerate irreversible thermal degradation of organic HTLs and QD ligands. To resolve this issue, Sun et al. employed a sapphire substrate with high thermal conductivity of $46 \text{ W m}^{-1} \text{ K}^{-1}$ and a thermally stable ligand, 1-dodecanethiol [12]. As a result, a high current efficiency of 75.3 cd A^{-1} and maximum luminance of $1,680,000 \text{ cd m}^{-2}$ have been achieved in a green QLED. Recently, Lee et al. also demonstrated highly bright and stable QLED using a Si/SiO₂ substrate with high thermal conductivity of $\sim 150 \text{ W m}^{-1} \text{ K}^{-1}$ [123], as shown in Figure 4c. Based on additional device optimization, the QLED on the Si-based substrate exhibited a current efficiency and maximum luminance of 75.6 cd A^{-1} and $3,300,000 \text{ cd m}^{-2}$, respectively.

3.3. QD Patterning Technologies

In order to realize AM-QLEDs, the QD layer should be formed in each individual subpixel. For this, QD patterning technologies have been investigated to comply with the requirements depending on the types of display application in terms of size, resolution, and the number of colors. In this section, we briefly introduce a few methodologies for QD patterning, such as contact printing, inkjet printing, photolithography, and light-induced direct QD patterning, and their pros and cons.

First, contact printing or contact transfer printing is one of the simplest patterning methods using an elastic stamp. A QD film deposited on a pre-patterned stamp can be transferred onto a target surface by using the difference of adhesion. In 2008, Kim et al. first reported a contact-printed QLED with a resolution of 1000 pixels-per-inch (PPI) using a Parylene-C-coated poly(dimethylsiloxane) (PDMS) stamp to control the surface energy and to prevent it from swirling by the QD solvent [128]. In 2011, Kim et al. introduced a self-assembled monolayer on the master substrate for easier detachment of the QD film and demonstrated a full-color AM-QLED [18]. Contact printing requires a high pressure to assure the transfer of QDs, and thus it is likely to damage the underlying layers and the transferred QD layer as well. In 2015, Cho et al. developed a soft contact QD transplanting technique, enabling the transfer of a QD layer onto a soft organic layer

without pressure [129], as shown in the Figure 5a. Nevertheless, contact printing with a stamp is not desired in the industry because of several issues in printing accuracy, stamp reliability, limited printable area, and non-uniformity.

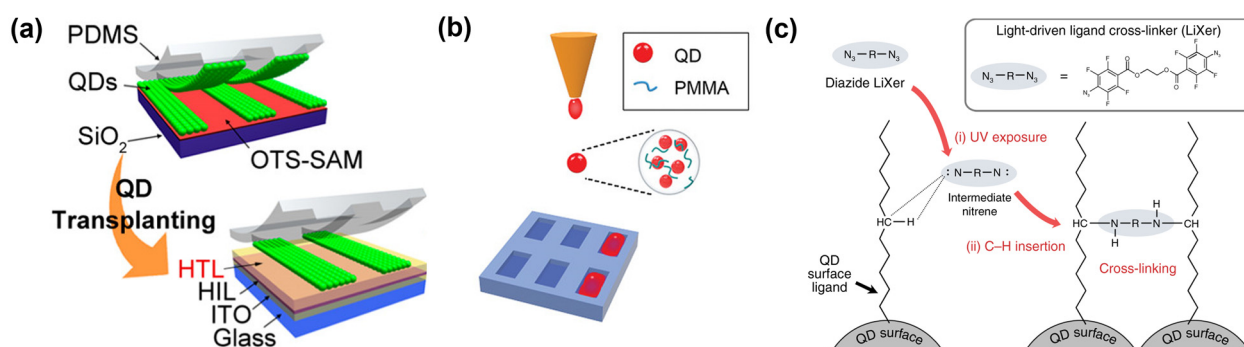


Figure 5. Schematic illustration of various QD patterning methods: (a) Contact transfer printing of QDs using a PDMS stamp (Reproduced from [129] with permission from American Chemical Society). (b) Inkjet printing of QD solution into subpixels (Reproduced from [130] with permission from Wiley). (c) UV-induced ligand crosslinking process for direct patterning of the QD film (Reproduced from [131] with permission from Springer Nature).

As a promising patterning technology, particularly for full-color AM-QLED displays, inkjet printing is attracting great attention from both academia and industry, owing to its high accuracy and low material usage based on drop-on-demand, and high throughput for large-area printing. On the other hand, poor film morphology is a weakness of inkjet printing. Inkjet-printed film morphology is related to several factors, such as the boiling point and vapor pressure of the solvent, the viscosity of ink, the surface energy of the substrate, and drying conditions. In most early-stage inkjet-printed QLEDs [132–134], the efficiency and brightness were relatively lower than those of the spin-coated QLED devices, mainly attributed to the poor QD morphology. Several strategies have been introduced to overcome this issue, such as using co-solvents to tune the boiling point and vapor pressure, mixing additives to control the viscosity, and substrate surface treatment to enhance wettability [130,135–140]. The Marangoni and capillary forces in a droplet can be optimized using these techniques to obtain a high-quality film. For example, Roh et al. reported QD–PMMA composite inks in a co-solvent to control the aforementioned key parameters and inkjet printing of fine QD films [130], as shown in Figure 5b. A ternary ink system consisting of octane, 1-cyclohexyl-ethanol, and n-butyl acetate was adopted to improve the morphology of QD film [15]. Recent intensive research on inkjet-printed QLEDs combined with device engineering has brought the inkjet-printed QLED performance to a level comparable to spin-coated ones [108,130,140,141], which should ease the commercialization of QLED displays.

Traditional photolithography can also be applied to pattern each QD subpixel. This matured technology provides a few advantages, such as high-resolution patterning and compatibility with the backplane fabrication procedure. However, there are several problems, for instance, physical damage to underlying QD and organic layers during photoresist (PR) deposition, development and removal processes, degradation of QDs by UV exposure, and defect formation from PR residues. Although full-color, high-resolution QLEDs could be demonstrated based on photolithography, the procedure to minimize the damages is exceedingly complicated [142,143]. Recently, a direct QD patterning method has been reported, which is a technique for patterning QDs based on photolithography but without the PR processes [131,144–148]. It can be achieved by adopting light-responsive ligands onto the surface of QDs, which chemically binds QDs upon illumination to firmly hold the pattern against the following wash-out step.

Specifically, in 2020, Cho et al. introduced direct optical lithography based QLEDs by employing photosensitive surface ligands, showing selective, full-color QD patterning

with a small feature size of $\sim 1.5 \mu\text{m}$ [146]. Yang et al. also reported a QD direct patterning method using a light-driven ligand crosslinker [131]. UV exposure to the modified QD film induces a chemical reaction between azides and the alkyl chain of QD ligands, resulting in a crosslinked QD layer, as shown in Figure 5c. Full-color, high-resolution QD patterns of >1400 PPI were demonstrated, and red crosslinked QLEDs exhibited an EQE of 14.6%. In 2022, Hahm et al. proposed direct patterning with dual ligands composed of dispersing ligands and photo-cross-linkable ligands to maintain the PL QY during photo-crosslinking [148]. As a result, they successfully demonstrated full-color QLED arrays employing the patterned QD films in a high resolution of >15000 PPI without a performance loss. Nevertheless, both traditional and direct photolithography requires a conventional UV lithography system for alignment and UV exposure, and thereby the processible substrates that can be processed are limited in size to the current wafer scale (300 mm). Thus, it is expected to be narrowly utilized for small-sized, high-resolution display devices, such as augmented/virtual reality (AR/VR) display devices.

Above and beyond these technologies, more QD patterning technologies, such as 3D printing [149,150], electrohydrodynamic printing [151], phase separation [152], electrophoretic deposition [153], and spatial light-assisted surface tailoring [154], have been introduced. However, these technologies are not suitable for implementing high-resolution displays and multilayer stacking or require complicated processes. Instead, we think that these technologies can be used in other ways, for instance, the fabrication of a QD color conversion layer for low-resolution displays or small lighting devices.

4. Monolithically Integrated TFT-QLED Devices

In Sections 2 and 3, we reviewed the development of TFT and QLED devices, respectively, in terms of circuitry design and electrical requirements for reliable AM driving. However, monolithic integration of TFT-QLED requires the use of compatible processes to achieve high performance for both devices in a concise and effective TFT-QLED design with a tolerable fabrication procedure to each other. Thus, we think that it is important to investigate the fabrication process, optical and electrical properties, and any possible combinational issues in monolithically integrated TFT-QLED devices.

As reviewed above, an oxide TFT is one of the promising backplane devices, as already used in the industry. They also have large-area processability and high electrical performance sufficient to drive QLEDs. Recently, Chen et al. showed that the luminance of an inverted QLED could be competently controlled by an IGZO TFT [26]. In particular, they developed Al reaction-induced conductive a-IGZO as a common electrode, exhibiting a low sheet resistance ($120 \Omega \text{sq}^{-1}$) and a high transmittance (92.1%), demonstrating reduced photolithographic mask steps as well as higher power efficiency at the same time. In 2019, Li et al. showed QLED arrays integrated on inkjet-printed InGaO TFTs [24], which is suitable for large-area AM-QLED fabrication. To improve the quality of inkjet-printed oxides, they adopted a solvent printing method and demonstrated red-emitting QLED arrays driven by a 2T1C circuit, as shown in Figure 6a.

Owing to the remarkable development of TFTs using TMDCs as an active material, integration of the TMDC-based TFTs with QLEDs has been presented gradually. In 2019, Roh et al. reported an enhancement-mode n-type MoS_2 TFT by octadecyltrichlorosilane (ODTS) SAM treatment to drive inverted QLEDs [23], as shown in Figure 6b. A deep-seated problem in depletion-mode TFTs is the large gate overdrive voltage ensuing rapid degradation of the channel. But the ODTS SAM enabled MoS_2 TFTs to operate in an enhancement mode, leading to depopulate electrons on the back channel. As a result, they showed a wide-range operation of the QLEDs by controlling V_T . In 2021, Baek et al. also demonstrated the stable operation of QLEDs driven by an integrated type convertible MoTe_2 TFT [25], as shown in Figure 6c. In particular, they showed that the TFT-QLED integrated device exhibits a negligible response to visible light and a fast response time utilizing the properties of the MoTe_2 channel. Also, a type-convertibility of the TFTs by

simple poly-L-lysine (PLL) treatment was demonstrated, which allows using both normal and inverted structures of QLEDs.

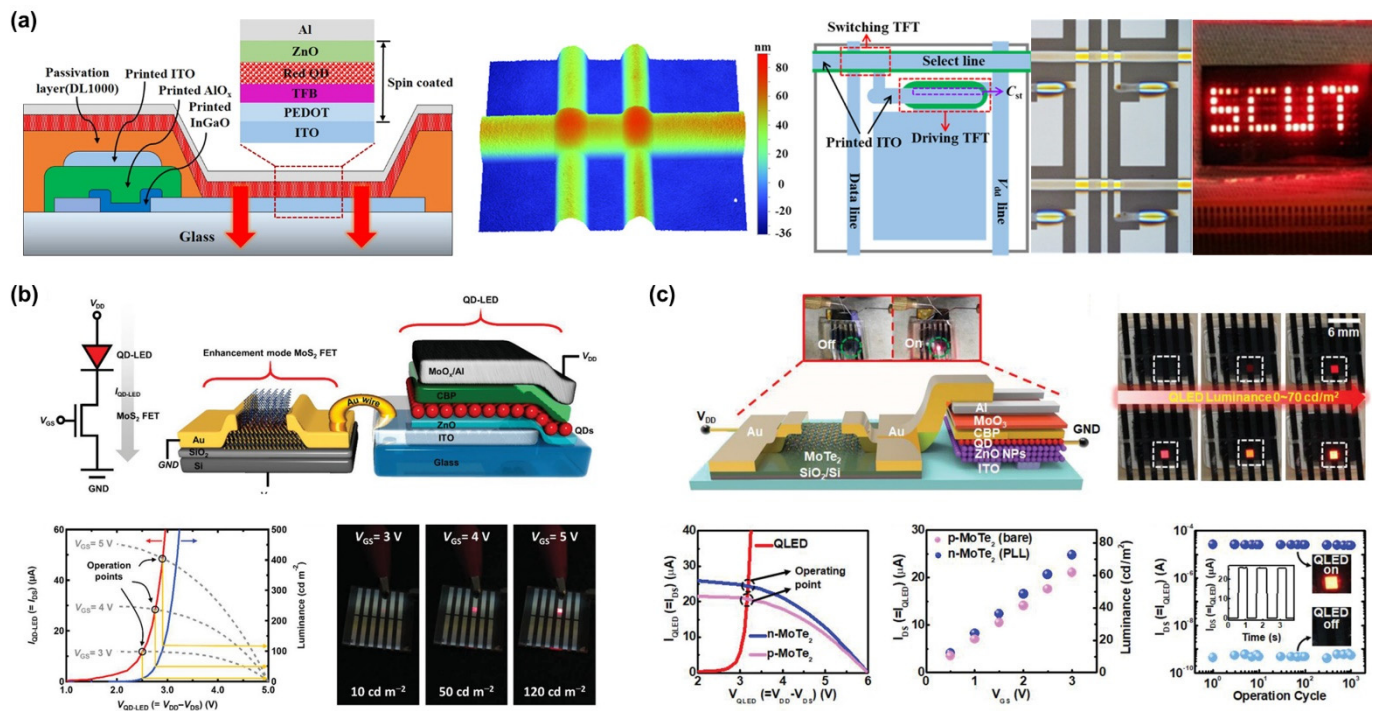


Figure 6. Monolithically integrated TFT-QLED devices: (a) Schematic cross-sectional diagram of inkjet-printed TFT-QLED pixel, the morphology of the inkjet-printed oxide film, the pixel structure, and a demonstration of the 2T1C-structured AM-QLED (Reproduced from [24] with permission from American Chemical Society). (b) Schemes of TFT-QLED using the multilayered MoS₂ TFT with ODTs-SAM on the back channel, current-voltage characteristics along with the driving current level, and luminance change (Reproduced from [23] with permission from Wiley). (c) Schematic structure of MoTe₂ TFT-driven QLED with luminance changes, current-voltage-luminance characteristics of type-converted TFTs via PLL treatment, current-voltage-luminance characteristics of the TFT-QLED device, and their stability (Reproduced from [25] with permission from Wiley).

As reviewed in this section, the research on TFT-QLED integrated devices is in its early stages but is gradually on the increase. The development of AM-QLED should be accompanied by not only respective performance improvement of the TFT backplane and QLED frontplane but also the requirements for monolithically integration in terms of circuitry design, the proper combination of TFT-QLED, and facile fabrication method. Such interest and intensive research would contribute to overcoming the known issues and limitations in regard to the fabrication process and reliability, enabling the realization of AM-QLEDs with advanced features.

5. Conclusions

In this review, we presented the fundamentals, state-of-the-art performance, and prospects of non-Si-based TFTs, QLEDs, and their combined forms, to achieve AM-QLED displays. As channel materials of the backplane TFT, metal oxides, TMDCs, and semiconducting SWNTs were considered to provide the requirements (e.g., high current driving, small V_T shift under BTS) for future display devices. Their new features against Si, such as solution-processability, light-insensitivity, flexibility, and transparency, may lead to a strong chance of success in a display application, although there still exist several issues (e.g., performance, stability, and solution-based fine patterning) which need to be resolved. Examination of QLEDs from the viewpoint of device architecture, device engineering, and QD patterning is also meaningful, giving a new prospective on the future research direction. Al-

though the QLEDs have been improved continuously, it is required to further develop more stable devices based on Cd-free QDs. In addition, the performance of pixelated QLEDs needs to be enhanced more. Finally, we reviewed the monolithic integration of TFT-QLED devices with the findings and issues toward AM-QLEDs. By solving the present issues, TFT-driven AM-QLEDs can be widely used as the main display panel with the advantages of a wide color gamut, high brightness, and low power consumption, which would expand the practical use from mobile devices and TVs to outdoor displays and AR/VR devices. We believe that this comprehensive review would be a valuable and inspiring guide for the readers in their future research with a wider perspective on AM-QLED displays.

Funding: This work was supported by the Creative-Pioneering Researchers Program through Seoul National University, by the Technology Innovation Program (20010737 and 20016332) funded by the Korean government (MOTIE), and by the National Research Foundation of Korea (NRF) grant (No. 2021R1A4A3032027) funded by the Korean government (MSIT).

Institutional Review Board Statement: Not applicable.

Informed Consent Statement: Not applicable.

Data Availability Statement: Not applicable.

Conflicts of Interest: The authors declare no conflict of interest.

References

1. Aroutiounian, V.; Petrosyan, S.; Khachatryan, A.; Touryan, K. Quantum Dot Solar Cells. *J. Appl. Phys.* **2001**, *89*, 2268–2271. [[CrossRef](#)]
2. Nozik, A.J. Quantum Dot Solar Cells. *Phys. E Low-Dimens. Syst. Nanostruct.* **2002**, *14*, 115–120. [[CrossRef](#)]
3. Semonin, O.E.; Nozik, A.J.; Beard, M.C. In a Quantum Dot Solar Cell. *Science* **2013**, *1530*, 1530–1534.
4. Shirasaki, Y.; Supran, G.J.; Bawendi, M.G.; Bulović, V. Emergence of Colloidal Quantum-Dot Light-Emitting Technologies. *Nat. Photonics* **2013**, *7*, 13–23. [[CrossRef](#)]
5. Kim, M.R.; Ma, D. Quantum-Dot-Based Solar Cells: Recent Advances, Strategies, and Challenges. *J. Phys. Chem. Lett.* **2015**, *6*, 85–99. [[CrossRef](#)]
6. Kim, T.H.; Lee, C.S.; Kim, S.; Hur, J.; Lee, S.; Shin, K.W.; Yoon, Y.Z.; Choi, M.K.; Yang, J.; Kim, D.H.; et al. Fully Stretchable Optoelectronic Sensors Based on Colloidal Quantum Dots for Sensing Photoplethysmographic Signals. *ACS Nano* **2017**, *11*, 5992–6003. [[CrossRef](#)] [[PubMed](#)]
7. Kim, J.; Shim, H.J.; Yang, J.; Choi, M.K.; Kim, D.C.; Kim, J.; Hyeon, T.; Kim, D.H. Ultrathin Quantum Dot Display Integrated with Wearable Electronics. *Adv. Mater.* **2017**, *29*, 1700217. [[CrossRef](#)]
8. Song, J.; Wang, O.; Shen, H.; Lin, Q.; Li, Z.; Wang, L.; Zhang, X.; Li, L.S. Over 30% External Quantum Efficiency Light-Emitting Diodes by Engineering Quantum Dot-Assisted Energy Level Match for Hole Transport Layer. *Adv. Funct. Mater.* **2019**, *29*, 1808377. [[CrossRef](#)]
9. Livache, C.; Martinez, B.; Goubet, N.; Gréboval, C.; Qu, J.; Chu, A.; Royer, S.; Ithurria, S.; Silly, M.G.; Dubertret, B.; et al. A Colloidal Quantum Dot Infrared Photodetector and Its Use for Intraband Detection. *Nat. Commun.* **2019**, *10*, 2125. [[CrossRef](#)]
10. Yin, X.; Zhang, C.; Guo, Y.; Yang, Y.; Xing, Y.; Que, W. PbS QD-based photodetectors: Future-oriented near-infrared detection technology. *J. Mater. Chem. C* **2021**, *9*, 417–438. [[CrossRef](#)]
11. Li, Z.; Hu, Y.; Shen, H.; Lin, Q.; Wang, L.; Wang, H.; Zhao, W.; Li, L.S. Efficient and Long-Life Green Light-Emitting Diodes Comprising Tridentate Thiol Capped Quantum Dots. *Laser Photonics Rev.* **2017**, *11*, 1600227. [[CrossRef](#)]
12. Sun, Y.; Su, Q.; Zhang, H.; Wang, F.; Zhang, S.; Chen, S. Investigation on Thermally Induced Efficiency Roll-Off: Toward Efficient and Ultrabright Quantum-Dot Light-Emitting Diodes. *ACS Nano* **2019**, *13*, 11433–11442. [[CrossRef](#)] [[PubMed](#)]
13. Li, Y.F.; Chou, S.Y.; Huang, P.; Xiao, C.; Liu, X.; Xie, Y.; Zhao, F.; Huang, Y.; Feng, J.; Zhong, H.; et al. Stretchable Organometal-Halide-Perovskite Quantum-Dot Light-Emitting Diodes. *Adv. Mater.* **2019**, *31*, 1807516. [[CrossRef](#)]
14. Kim, T.; Kim, K.H.; Kim, S.; Choi, S.M.; Jang, H.; Seo, H.K.; Lee, H.; Chung, D.Y.; Jang, E. Efficient and stable blue quantum dot light-emitting diode. *Nature* **2020**, *586*, 385–389. [[CrossRef](#)]
15. Jia, S.; Tang, H.; Ma, J.; Ding, S.; Qu, X.; Xu, B.; Wu, Z.; Li, G.; Liu, P.; Wang, K.; et al. High Performance Inkjet-Printed Quantum-Dot Light-Emitting Diodes with High Operational Stability. *Adv. Opt. Mater.* **2021**, *9*, 2101069. [[CrossRef](#)]
16. Chao, W.C.; Chiang, T.H.; Liu, Y.C.; Huang, Z.X.; Liao, C.C.; Chu, C.H.; Wang, C.H.; Tseng, H.W.; Hung, W.Y.; Chou, P.T. High efficiency green InP quantum dot light-emitting diodes by balancing electron and hole mobility. *Commun. Mater.* **2021**, *2*, 96. [[CrossRef](#)]
17. Cho, K.S.; Lee, E.K.; Joo, W.J.; Jang, E.; Kim, T.H.; Lee, S.J.; Kwon, S.J.; Han, J.Y.; Kim, B.K.; Choi, B.L.; et al. High-performance crosslinked colloidal quantum-dot light-emitting diodes. *Nat. Photonics* **2009**, *3*, 341–345. [[CrossRef](#)]

18. Kim, T.H.; Cho, K.S.; Lee, E.K.; Lee, S.J.; Chae, J.; Kim, J.W.; Kim, D.H.; Kwon, J.Y.; Amaratunga, G.; Lee, S.Y.; et al. Full-colour quantum dot displays fabricated by transfer printing. *Nat. Photonics* **2011**, *5*, 176–182. [[CrossRef](#)]
19. Yang, Y.; Zheng, Y.; Cao, W.; Titov, A.; Hyvonen, J.; Manders, J.R.; Xue, J.; Holloway, P.H.; Qian, L. High-efficiency light-emitting devices based on quantum dots with tailored nanostructures. *Nat. Photonics* **2015**, *9*, 259–265. [[CrossRef](#)]
20. Lai, K.Y.; Yang, S.; Tsai, T.C.; Yao, I.A.; Yang, C.L.; Chang, C.C.; Chen, H.S. Top-Emitting Active-Matrix Quantum Dot Light-Emitting Diode Array with Optical Microcavity for Micro QLED Display. *Nanomaterials* **2022**, *12*, 2683. [[CrossRef](#)]
21. Jiang, C.; Mu, L.; Zou, J.; He, Z.; Zhong, Z.; Wang, L.; Xu, M.; Wang, J.; Peng, J.; Cao, Y. Full-Color Quantum Dots Active Matrix Display Fabricated by Ink-Jet Printing. *Sci. China Chem.* **2017**, *60*, 1349–1355. [[CrossRef](#)]
22. Li, Y.; Chen, Z.; Kristal, B.; Zhang, Y.; Li, D.; Yu, G.; Wang, X.; Wang, L.; Shi, Y.; Wang, Z.; et al. Developing AMQLED Technology for Display Applications. *SID Int. Symp. Dig. Tech. Pap.* **2018**, *49*, 1076–1079. [[CrossRef](#)]
23. Roh, J.; Ryu, J.H.; Baek, G.W.; Jung, H.; Seo, S.G.; An, K.; Jeong, B.G.; Lee, D.C.; Hong, B.H.; Bae, W.K.; et al. Threshold Voltage Control of Multilayered MoS₂ Field-Effect Transistors via Octadecyltrichlorosilane and Their Applications to Active Matrixed Quantum Dot Displays Driven by Enhancement-Mode Logic Gates. *Small* **2019**, *15*, 1803852. [[CrossRef](#)] [[PubMed](#)]
24. Li, Y.; He, P.; Chen, S.; Lan, L.; Dai, X.; Peng, J. Inkjet-Printed Oxide Thin-Film Transistors Based on Nanopore-Free Aqueous-Processed Dielectric for Active-Matrix Quantum-Dot Light-Emitting Diode Displays. *ACS Appl. Mater. Interfaces* **2019**, *11*, 28052–28059. [[CrossRef](#)]
25. Baek, G.W.; Seo, S.G.; Hahm, D.; Bae, W.K.; Kwak, J.; Jin, S.H. Highly Efficient, Surface Ligand Modified Quantum Dot Light-Emitting Diodes Driven by Type-Controllable MoTe₂ Thin Film Transistors via Electron Charge Enhancer. *Adv. Electron. Mater.* **2021**, *7*, 2100535. [[CrossRef](#)]
26. Chen, C.; Su, S.; Zhang, S.; Chen, S. Al Reaction-Induced Conductive a-InGaZnO as Pixel Electrode for Active-Matrix Quantum-Dot LED Displays. *IEEE Electron Device Lett.* **2022**, *43*, 749–752. [[CrossRef](#)]
27. Jin, S.H.; Kang, S.K.; Cho, I.T.; Han, S.Y.; Chung, H.U.; Lee, D.J.; Shin, J.; Baek, G.W.; Kim, T.; Lee, J.H.; et al. Water-Soluble Thin Film Transistors and Circuits Based on Amorphous Indium-Gallium-Zinc Oxide. *ACS Appl. Mater. Interfaces* **2015**, *7*, 8268–8274. [[CrossRef](#)]
28. Ryu, J.H.; Baek, G.W.; Yu, S.J.; Seo, S.G.; Jin, S.H. Photosensitive Full-Swing Multi-Layer MoS₂ inverters with Light Shielding Layers. *IEEE Electron Device Lett.* **2017**, *38*, 67–70. [[CrossRef](#)]
29. Choi, M.; Park, Y.J.; Sharma, B.K.; Bae, S.R.; Kim, S.Y.; Ahn, J.H. Flexible Active-Matrix Organic Light-Emitting Diode Display Enabled by MoS₂ Thin-Film Transistor. *Sci. Adv.* **2018**, *4*, eaas8721. [[CrossRef](#)]
30. Choi, M.; Bae, S.R.; Hu, L.; Hoang, A.T.; Kim, S.Y.; Ahn, J.H. Full-Color Active-Matrix Organic Light-Emitting Diode Display on Human Skin Based on a Large-Area MoS₂ backplane. *Sci. Adv.* **2020**, *6*, eabb5898. [[CrossRef](#)]
31. Khan, M.I.; Baek, G.W.; Kim, K.; Jin, S.H. Simultaneous Detection of Dopamine and Uric Acid on Indium Tin Oxides Modified with Cost-Effective Gas-Phase Synthesized Single Walled Carbon Nanotubes. *Electroanalysis* **2017**, *29*, 1925–1933. [[CrossRef](#)]
32. Kim, J.; Lee, J.; Jang, J. AMQLED Display with Solution-Processed Oxide TFT Backplane. *SID Int. Symp. Dig. Tech. Pap.* **2018**, *49*, 1080–1083. [[CrossRef](#)]
33. Srivastava, A.; Dubey, D.; Goswami, M.; Kandpal, K. Mechanical Strain and Bias-Stress Compensated, 6T-1C Pixel Circuit for Flexible AMOLED Displays. *Microelectron. J.* **2021**, *117*, 105266. [[CrossRef](#)]
34. Wu, W.J.; Zhou, L.; Yao, R.H.; Peng, J.B. A New Voltage-Programmed Pixel Circuit for Enhancing the Uniformity of AMOLED Displays. *IEEE Electron Device Lett.* **2011**, *32*, 931–933. [[CrossRef](#)]
35. Bang, J.S.; Kim, H.S.; Kim, K.D.; Kwon, O.J.; Shin, C.S.; Lee, J.; Cho, G.H. A Hybrid AMOLED Driver IC for Real-Time TFT Nonuniformity Compensation. *IEEE J. Solid-State Circuits* **2016**, *51*, 966–978.
36. Lin, C.L.; Chang, W.Y.; Hung, C.C. Compensating Pixel Circuit Driving AMOLED Display with A-IGZO TFTs. *IEEE Electron Device Lett.* **2013**, *34*, 1166–1168. [[CrossRef](#)]
37. Park, J.H.; Seok, H.J.; Kim, C.H.; Jung, S.H.; Cho, H.K.; Kim, H.K. Compositional Engineering of Hf-Doped InZnSnO Films for High-Performance and Stability Amorphous Oxide Semiconductor Thin Film Transistors. *Adv. Electron. Mater.* **2021**, *7*, 2001216. [[CrossRef](#)]
38. Jeong, H.J.; Lee, H.M.; Ryu, C.H.; Park, E.J.; Han, K.L.; Hwang, H.J.; Ok, K.C.; Kim, H.S.; Park, J.S. Ultra-High-Speed Intense Pulsed-Light Irradiation Technique for High-Performance Zinc Oxynitride Thin-Film Transistors. *ACS Appl. Mater. Interfaces* **2019**, *11*, 4152–4158. [[CrossRef](#)]
39. Chung, J.; Tak, Y.J.; Kim, W.G.; Park, J.W.; Kim, T.S.; Lim, J.H.; Kim, H.J. Low-Temperature Fabrication of Solution-Processed Hafnium Oxide Gate Insulator Films Using a Thermally Purified Solution Process. *J. Mater. Chem. C* **2018**, *6*, 4928–4935. [[CrossRef](#)]
40. Park, E.J.; Lee, H.M.; Kim, Y.S.; Jeong, H.J.; Park, J.; Park, J.S. Transparent Flexible High Mobility TFTs Based on ZnON Semiconductor with Dual Gate Structure. *IEEE Electron Device Lett.* **2020**, *41*, 401–404. [[CrossRef](#)]
41. Yang, J.; Zhang, Y.; Wu, Q.; Dussarrat, C.; Qi, J.; Zhu, W.; Ding, X.; Zhang, J. High-Performance 1-V ZnO Thin-Film Transistors with Ultrathin, ALD-Processed ZrO₂ Gate Dielectric. *IEEE Trans. Electron Devices* **2019**, *66*, 3382–3386. [[CrossRef](#)]
42. Ren, J.; Li, K.; Yang, J.; Lin, D.; Kang, H.; Shao, J.; Fu, R.; Zhang, Q. Solution-Processed Amorphous Gallium-Tin Oxide Thin Film for Low-Voltage, High-Performance Transistors. *Sci. China Mater.* **2019**, *62*, 803–812. [[CrossRef](#)]
43. Magari, Y.; Kataoka, T.; Yeh, W.; Furuta, M. High-Mobility Hydrogenated Polycrystalline In₂O₃ (In₂O₃:H) Thin-Film Transistors. *Nat. Commun.* **2022**, *13*, 1078. [[CrossRef](#)] [[PubMed](#)]

44. Li, Y.; Liu, C.; Wang, G.; Pei, Y. Investigation of Solution Combustion- Processed Nickel Oxide p-Channel Thin Film Transistors. *Semicond. Sci. Technol.* **2017**, *32*, 085004. [[CrossRef](#)]
45. Liang, L.Y.; Liu, Z.M.; Cao, H.T.; Yu, Z.; Shi, Y.Y.; Chen, A.H.; Zhang, H.Z.; Fang, Y.Q.; Sun, X.L. Phase and Optical Characterizations of Annealed SnO Thin Films and Their P-Type TFT Application. *J. Electrochem. Soc.* **2010**, *157*, H598. [[CrossRef](#)]
46. Sanal, K.C.; Vikas, L.S.; Jayaraj, M.K. Room Temperature Deposited Transparent P-Channel CuO Thin Film Transistors. *Appl. Surf. Sci.* **2014**, *297*, 153–157. [[CrossRef](#)]
47. Ryu, J.H.; Baek, G.W.; Kim, S.Y.; Kwon, H.I.; Jin, S.H. Spray-Coated Single Walled Carbon Nanotubes as Source and Drain Electrodes in SnO Thin-Film Transistors. *Semicond. Sci. Technol.* **2018**, *33*, 075013. [[CrossRef](#)]
48. Liu, N.; Baek, J.; Kim, S.M.; Hong, S.; Hong, Y.K.; Kim, Y.S.; Kim, H.S.; Kim, S.; Park, J. Improving the Stability of High-Performance Multilayer MoS₂ Field-Effect Transistors. *ACS Appl. Mater. Interfaces* **2017**, *9*, 42943–42950. [[CrossRef](#)]
49. Li, N.; Wang, Q.; Shen, C.; Wei, Z.; Yu, H.; Zhao, J.; Lu, X.; Wang, G.; He, C.; Xie, L.; et al. Large-Scale Flexible and Transparent Electronics Based on Monolayer Molybdenum Disulfide Field-Effect Transistors. *Nat. Electron.* **2020**, *3*, 711–717. [[CrossRef](#)]
50. Zhu, K.; Wen, C.; Aljarb, A.A.; Xue, F.; Xu, X.; Tung, V.; Zhang, X.; Alshareef, H.N.; Lanza, M. The Development of Integrated Circuits Based on Two-Dimensional Materials. *Nat. Electron.* **2021**, *4*, 775–785. [[CrossRef](#)]
51. Zhao, Y.; Song, Y.; Hu, Z.; Wang, W.; Chang, Z.; Zhang, Y.; Lu, Q.; Wu, H.; Liao, J.; Zou, W.; et al. Large-Area Transfer of Two-Dimensional Materials Free of Cracks, Contamination and Wrinkles via Controllable Conformal Contact. *Nat. Commun.* **2022**, *13*, 4409. [[CrossRef](#)] [[PubMed](#)]
52. Tans, S.J.; Verschueren, A.R.M.; Dekker, C. Room-Temperature Transistor Based on a Single Carbon Nanotube. *Nature* **1998**, *393*, 49–52. [[CrossRef](#)]
53. Artukovic, E.; Kaempgen, M.; Hecht, D.S.; Roth, S.; Grüner, G. Transparent and Flexible Carbon Nanotube Transistors. *Nano Lett.* **2005**, *5*, 757–760. [[CrossRef](#)] [[PubMed](#)]
54. Sun, D.; Timmermans, M.Y.; Tian, Y.; Nasibulin, A.G.; Kauppinen, E.I.; Kishimoto, S.; Mizutani, T.; Ohno, Y. Flexible High-Performance Carbon Nanotube Integrated Circuits. *Nat. Nanotechnol.* **2011**, *6*, 156–161. [[CrossRef](#)] [[PubMed](#)]
55. Sun, D.; Liu, C.; Ren, W.; Cheng, H. A Review of Carbon Nanotube- and Graphene-Based Flexible Thin-Film Transistors. *Small* **2013**, *9*, 1188–1205. [[CrossRef](#)] [[PubMed](#)]
56. Liu, H.; Nishide, D.; Tanaka, T.; Kataura, H. Large-Scale Single-Chirality Separation of Single-Wall Carbon Nanotubes by Simple Gel Chromatography. *Nat. Commun.* **2011**, *2*, 309. [[CrossRef](#)]
57. Tanaka, T.; Liu, H.; Fujii, S.; Kataura, H. From Metal/Semiconductor Separation to Single-chirality Separation of Single-wall Carbon Nanotubes Using Gel. *Phys. Status Solidi-Rapid Res. Lett.* **2011**, *5*, 301–306. [[CrossRef](#)]
58. Rojas, W.A.G.; Hersam, M.C. Chirality-Enriched Carbon Nanotubes for Next-Generation Computing. *Adv. Mater.* **2020**, *32*, 1905654. [[CrossRef](#)]
59. Tu, X.; Zheng, M. A DNA-Based Approach to the Carbon Nanotube Sorting Problem. *Nano Res.* **2008**, *1*, 185–194. [[CrossRef](#)]
60. Asada, Y.; Miyata, Y.; Ohno, Y.; Kitaura, R.; Sugai, T.; Mizutani, T.; Shinohara, H. High-Performance Thin-Film Transistors with DNA-Assisted Solution Processing of Isolated Single-Walled Carbon Nanotubes. *Adv. Mater.* **2010**, *22*, 2698–2701. [[CrossRef](#)]
61. Gomulya, W.; Gao, J.; Loi, M.A. Conjugated Polymer-Wrapped Carbon Nanotubes: Physical Properties and Device Applications. *Eur. Phys. J. B* **2013**, *86*, 404. [[CrossRef](#)]
62. Samanta, S.K.; Fritsch, M.; Scherf, U.; Gomulya, W.; Bisri, S.Z.; Loi, M.A. Conjugated Polymer-Assisted Dispersion of Single-Wall Carbon Nanotubes: The Power of Polymer Wrapping. *Acc. Chem. Res.* **2014**, *47*, 2446–2456. [[CrossRef](#)] [[PubMed](#)]
63. Chen, H.; Xing, X.; Zhu, M.; Cao, J.; Ali, M.U.; Li, A.; He, Y.; Meng, H. Low-Voltage, High-Performance Flexible Organic Field-Effect Transistors Based on Ultrathin Single-Crystal Microribbons. *ACS Appl. Mater. Interfaces* **2019**, *11*, 34188–34195. [[CrossRef](#)] [[PubMed](#)]
64. Peng, B.; Ji, X.; Jiao, X.; Chu, M.; Liu, J.; Li, Y.; Chen, M.; Zhou, Z.; Zhang, C.; Miao, Q.; et al. A Transfer Method for High-Mobility, Bias-Stable, and Flexible Organic Field-Effect Transistors. *Adv. Mater. Technol.* **2020**, *5*, 2000169. [[CrossRef](#)]
65. Han, M.J.; Lee, D.W.; Lee, E.K.; Kim, J.Y.; Jung, J.Y.; Kang, H.; Ahn, H.; Shin, T.J.; Yoon, D.K.; Park, J. II Molecular Orientation Control of Liquid Crystal Organic Semiconductor for High-Performance Organic Field-Effect Transistors. *ACS Appl. Mater. Interfaces* **2021**, *13*, 11125–11133. [[CrossRef](#)]
66. Haase, K.; Teixeira da Rocha, C.; Hauenstein, C.; Zheng, Y.; Hambsch, M.; Mannsfeld, S.C.B. High-Mobility, Solution-Processed Organic Field-Effect Transistors from C8-BTBT:Polystyrene Blends. *Adv. Electron. Mater.* **2018**, *4*, 1800076. [[CrossRef](#)]
67. Fu, B.; Sun, L.; Liu, L.; Ji, D.; Zhang, X.; Yang, F.; Hu, W. Low-Power High-Mobility Organic Single-Crystal Field-Effect Transistor. *Sci. China Mater.* **2022**, *65*, 2779–2785. [[CrossRef](#)]
68. Xia, G.; Zhang, Q.; Wang, S. High-Mobility IGZO TFTs by Infrared Radiation Activated Low-Temperature Solution Process. *IEEE Electron Device Lett.* **2018**, *39*, 1868–1871. [[CrossRef](#)]
69. Liu, Y.; Guo, J.; Zhu, E.; Liao, L.; Lee, S.-J.; Ding, M.; Shakir, I.; Gambin, V.; Huang, Y.; Duan, X. Approaching the Schottky–Mott Limit in van Der Waals Metal–Semiconductor Junctions. *Nature* **2018**, *557*, 696–700. [[CrossRef](#)]
70. Schneider, S.; Brohmann, M.; Lorenz, R.; Hofstetter, Y.J.; Rother, M.; Sauter, E.; Zharnikov, M.; Vaynzof, Y.; Himmel, H.-J.; Zaumseil, J. Efficient n-Doping and Hole Blocking in Single-Walled Carbon Nanotube Transistors with 1,2,4,5-Tetrakis(Tetramethylguanidino)Ben-Zene. *ACS Nano* **2018**, *12*, 5895–5902. [[CrossRef](#)]

71. Wang, Y.; Kim, J.C.; Wu, R.J.; Martinez, J.; Song, X.; Yang, J.; Zhao, F.; Mkhoyan, A.; Jeong, H.Y.; Chhowalla, M. Van Der Waals Contacts between Three-Dimensional Metals and Two-Dimensional Semiconductors. *Nature* **2019**, *568*, 70–74. [[CrossRef](#)] [[PubMed](#)]
72. Zhang, Z.; Zhang, M.; Du, C.; Li, L.; Chang, K.-C. Improving Performance of All-Carbon-Nanotube Thin-Film Transistors by Low Temperature Supercritical CO₂ Fluid Activation. *IEEE Electron Device Lett.* **2019**, *40*, 921–924. [[CrossRef](#)]
73. Sanjay, S.; Sahoo, K.; Bhat, N. Alcohol-Based Sulfur Treatment for Improved Performance and Yield in Local Back-Gated and Channel-Length-Scaled MoS₂ FETs. *IEEE Trans. Electron Devices* **2020**, *67*, 3711–3715. [[CrossRef](#)]
74. Salazar-Rios, J.M.; Sengrian, A.A.; Talsma, W.; Duim, H.; Abdu-Aguye, M.; Jung, S.; Fröhlich, N.; Allard, S.; Scherf, U.; Loi, M.A. Customizing the Polarity of Single-Walled Carbon-Nanotube Field-Effect Transistors Using Solution-Based Additives. *Adv. Electron. Mater.* **2020**, *6*, 1900789. [[CrossRef](#)]
75. Iqbal, M.W.; Elahi, E.; Amin, A.; Aftab, S.; Aslam, I.; Hussain, G.; Shehzad, M.A. A Facile Route to Enhance the Mobility of MoTe₂ Field Effect Transistor via Chemical Doping. *Superlattices Microstruct.* **2020**, *147*, 106698. [[CrossRef](#)]
76. Kim, B.K.; On, N.; Choi, C.H.; Kim, M.J.; Kang, S.; Lim, J.H.; Jeong, J.K. Polycrystalline Indium Gallium Tin Oxide Thin-Film Transistors with High Mobility Exceeding 100 cm²/Vs. *IEEE Electron Device Lett.* **2021**, *42*, 347–350. [[CrossRef](#)]
77. Kumar, S.; Sharma, A.; Tomar, M.; Gupta, V. Realization of Low-Power and High Mobility Thin Film Transistors Based on MoS₂ Layers Grown by PLD Technique. *Mater. Sci. Eng. B* **2021**, *266*, 115047. [[CrossRef](#)]
78. Kim, S.; Baek, G.W.; Jeong, J.; Seo, S.G.; Jin, S.H. Scalable and Selective N-Type Conversion for Carbon Nanotube Transistors via Patternable Polyvinyl Alcohol Stacked with Hydrophobic Layers and Their Application to Complementary Logic Circuits. *J. Mater. Res. Technol.* **2021**, *12*, 243–256. [[CrossRef](#)]
79. Seo, S.G.; Jeong, J.; Kim, S.Y.; Kim, S.; Kim, K.; Kim, K.; Jin, S.H. Bias Stress Instability in Multilayered MoTe₂ Field Effect Transistors under DC and Pulse-Mode Operation. *Electron. Lett.* **2021**, *57*, 193–195. [[CrossRef](#)]
80. Hwangbo, S.; Hu, L.; Hoang, A.T.; Choi, J.Y.; Ahn, J.-H. Wafer-Scale Monolithic Integration of Full-Colour Micro-LED Display Using MoS₂ Transistor. *Nat. Nanotechnol.* **2022**, *17*, 500–506. [[CrossRef](#)]
81. Sun, Y.; Li, P.; Kauppinen, E.I.; Sun, D.-M.; Ohno, Y. Key Factors for Ultra-High on/off Ratio Thin-Film Transistors Using as-Grown Carbon Nanotube Networks. *RSC Adv.* **2022**, *12*, 16291–16295. [[CrossRef](#)] [[PubMed](#)]
82. Huyen Nguyen, P.; Hieu Nguyen, D.; Kim, H.; Jeong, H.M.; Oh, H.M.; Jeong, M.S. Synergistic Hole-Doping on Ultrathin MoTe₂ for Highly Stable Unipolar Field-Effect Transistor. *Appl. Surf. Sci.* **2022**, *596*, 153567. [[CrossRef](#)]
83. Colvin, V.L.; Schlamp, M.C.; Alivisatos, A.P. Light-Emitting Diodes Made from Cadmium Selenide Nanocrystals and a Semiconducting Polymer. *Nature* **1994**, *370*, 354–357. [[CrossRef](#)]
84. Jang, H.J.; Lee, J.Y.; Baek, G.W.; Kwak, J.; Park, J.-H. Progress in the development of the display performance of AR, VR, QLED and OLED devices in recent years. *J. Inf. Disp.* **2022**, *23*, 1–17. [[CrossRef](#)]
85. Bae, W.K.; Kwak, J.; Lim, J.; Lee, D.; Nam, M.K.; Char, K.; Lee, C.; Lee, S. Multicolored light-emitting diodes based on all-quantum-dot multilayer films using layer-by-layer assembly method. *Nano Lett.* **2010**, *10*, 2368–2373. [[CrossRef](#)] [[PubMed](#)]
86. Kwak, J.; Bae, W.K.; Lee, D.; Park, I.; Lim, J.; Park, M.; Cho, H.; Woo, H.; Yoon, D.Y.; Char, K.; et al. Bright and efficient full-color colloidal quantum dot light-emitting diodes using an inverted device structure. *Nano Lett.* **2012**, *12*, 2362–2366. [[CrossRef](#)]
87. Qian, L.; Zheng, Y.; Choudhury, K.R.; Bera, D.; So, F.; Xue, J.; Holloway, P.H. Electroluminescence from Light-Emitting Polymer/ZnO Nanoparticle Heterojunctions at Sub-Bandgap Voltages. *Nano Today* **2010**, *5*, 384–389. [[CrossRef](#)]
88. Qian, L.; Zheng, Y.; Xue, J.; Holloway, P.H. Stable and Efficient Quantum-Dot Light-Emitting Diodes Based on Solution-Processed Multilayer Structures. *Nat. Photonics* **2011**, *5*, 543–548. [[CrossRef](#)]
89. Yang, X.; Mutlugun, E.; Dang, C.; Dev, K.; Gao, Y.; Tan, S.T.; Sun, X.W.; Demir, H.V. Highly flexible, electrically driven, top-emitting, quantum dot light-emitting stickers. *ACS Nano* **2014**, *8*, 8224–8231. [[CrossRef](#)]
90. Ding, K.; Fang, Y.; Dong, S.; Chen, H.; Luo, B.; Jiang, K.; Gu, H.; Fan, L.; Liu, S.; Hu, B.; et al. 24.1% External Quantum Efficiency of Flexible Quantum Dot Light-Emitting Diodes by Light Extraction of Silver Nanowire Transparent Electrodes. *Adv. Opt. Mater.* **2018**, *6*, 1800347. [[CrossRef](#)]
91. Li, D.; Feng, J.; Zhu, Y.; Lu, Z.; Pei, C.; Chen, Z.; Li, Y.; Li, X.; Xu, X. Enhanced efficiency of top-emission InP-based green quantum dot light-emitting diodes with optimized angular distribution. *Nano Research* **2021**, *14*, 4243–4249. [[CrossRef](#)]
92. Chen, L.; Qin, Z.; Chen, S. Ultrahigh Resolution Pixelated Top-Emitting Quantum-Dot Light-Emitting Diodes Enabled by Color-Converting Cavities. *Small Methods* **2022**, *6*, 2101090. [[CrossRef](#)] [[PubMed](#)]
93. Liu, G.; Zhou, X.; Chen, S. Very bright and efficient microcavity top-emitting quantum dot light-emitting diodes with Ag electrodes. *ACS Appl. Mater. Interfaces* **2016**, *8*, 16768–16775. [[CrossRef](#)] [[PubMed](#)]
94. Zhang, X.; Pan, T.; Zhang, J.; Zhang, L.; Liu, S.; Xie, W. Color-tunable, spectra-stable flexible white top-emitting organic light-emitting devices based on alternating current driven and dual-microcavity technology. *ACS Photonics* **2019**, *6*, 2350–2357. [[CrossRef](#)]
95. Yu, H.; Zhu, H.; Xu, M.; Zhang, J.; Feng, H.; Zhang, L.; Liu, S.; Xie, W. High-Efficiency, Large-Area, Flexible Top-Emitting Quantum-Dot Light-Emitting Diode. *ACS Photonics* **2022**. [[CrossRef](#)]
96. Shi, L.; Chen, S. Over 32.5% Efficient Top-Emitting Quantum-Dot LEDs with Angular-Independent Emission. *ACS Appl. Mater. Interfaces* **2022**, *14*, 30039–30045. [[CrossRef](#)]
97. Kim, H.-M.; Lee, J.; Hwang, E.; Kim, J.; Jang, J. P-95: Inverted tandem architecture of quantum-dot light emitting diodes with solution processed charge generation layers. *SID Int. Symp. Dig. Tech. Pap.* **2016**, *47*, 1480–1483. [[CrossRef](#)]

98. Zhang, H.; Sun, X.; Chen, S. Over 100 cd A⁻¹ efficient quantum dot light-emitting diodes with inverted tandem structure. *Adv. Funct. Mater.* **2017**, *27*, 1700610. [[CrossRef](#)]
99. Zhang, H.; Chen, S.; Sun, X.W. Efficient red/green/blue tandem quantum-dot light-emitting diodes with external quantum efficiency exceeding 21%. *ACS nano* **2018**, *12*, 697–704. [[CrossRef](#)]
100. Su, Q.; Zhang, H.; Chen, S. Flexible and tandem quantum-dot light-emitting diodes with individually addressable red/green/blue emission. *npj Flex. Electron.* **2021**, *5*, 8. [[CrossRef](#)]
101. Cho, S.-Y.; Oh, N.; Nam, S.; Jiang, Y.; Shim, M. Enhanced device lifetime of double-heterojunction nanorod light-emitting diodes. *Nanoscale* **2017**, *9*, 6103–6110. [[CrossRef](#)] [[PubMed](#)]
102. Yun, J.; Kim, J.; Jung, B.J.; Kim, G.; Kwak, J. Enhanced efficiency and high temperature stability of hybrid quantum dot light-emitting diodes using molybdenum oxide doped hole transport layer. *RSC Adv.* **2019**, *9*, 16252–16257. [[CrossRef](#)] [[PubMed](#)]
103. Bae, W.K.; Kwak, J.; Lim, J.; Lee, D.; Nam, M.K.; Char, K.; Lee, C.; Lee, S. Deep blue light-emitting diodes based on Cd_{1-x}Zn_xS@ZnS quantum dots. *Nanotechnology* **2009**, *20*, 075202. [[CrossRef](#)] [[PubMed](#)]
104. Li, Y.; Hou, X.; Dai, X.; Yao, Z.; Lv, L.; Jin, Y.; Peng, X. Stoichiometry-controlled InP-based quantum dots: Synthesis, photoluminescence, and electroluminescence. *J. Am. Chem. Soc.* **2019**, *141*, 6448–6452. [[CrossRef](#)]
105. Li, J.; Liang, Z.; Su, Q.; Jin, H.; Wang, K.; Xu, G.; Xu, X. Small molecule-modified hole transport layer targeting low turn-on-voltage, bright, and efficient full-color quantum dot light emitting diodes. *ACS Appl. Mater. Interfaces* **2018**, *10*, 3865–3873. [[CrossRef](#)]
106. Hong, A.; Kim, J.; Kwak, J. Sunlike White Quantum Dot Light-Emitting Diodes with High Color Rendition Quality. *Adv. Opt. Mater.* **2020**, *8*, 2001051. [[CrossRef](#)]
107. Yang, P.; Zhang, L.; Kang, D.J.; Strahl, R.; Kraus, T. High-resolution inkjet printing of quantum dot light-emitting microdiode arrays. *Adv. Opt. Mater.* **2020**, *8*, 1901429. [[CrossRef](#)]
108. Chen, M.; Xie, L.; Wei, C.; Yi, Y.-Q.-Q.; Chen, X.; Yang, J.; Zhuang, J.; Li, F.; Su, W.; Cui, Z. High performance inkjet-printed QLEDs with 18.3% EQE: Improving interfacial contact by novel halogen-free binary solvent system. *Nano Res.* **2021**, *14*, 4125–4131. [[CrossRef](#)]
109. Han, M.G.; Lee, Y.; Kwon, H.-i.; Lee, H.; Kim, T.; Won, Y.-H.; Jang, E. InP-based quantum dot light-emitting diode with a blended emissive layer. *ACS Energy Lett.* **2021**, *6*, 1577–1585. [[CrossRef](#)]
110. Zhang, Y.; Li, Z.; Wang, F.; Lin, Q.; Zhao, M. To improve the performance of green light-emitting devices by enhancing hole injection efficiency. *Chem. Eng. J. Adv.* **2021**, *5*, 100082. [[CrossRef](#)]
111. Lee, S.; Hahm, D.; Yoon, S.-Y.; Yang, H.; Bae, W.K.; Kwak, J. Quantum-dot and organic hybrid light-emitting diodes employing a blue common layer for simple fabrication of full-color displays. *Nano Res.* **2022**, *15*, 6477–6482. [[CrossRef](#)]
112. Li, X.; Zhao, Y.-B.; Fan, F.; Levina, L.; Liu, M.; Quintero-Bermudez, R.; Gong, X.; Quan, L.N.; Fan, J.; Yang, Z. Bright colloidal quantum dot light-emitting diodes enabled by efficient chlorination. *Nat. Photonics* **2018**, *12*, 159–164. [[CrossRef](#)]
113. Won, Y.-H.; Cho, O.; Kim, T.; Chung, D.-Y.; Kim, T.; Chung, H.; Jang, H.; Lee, J.; Kim, D.; Jang, E. Highly efficient and stable InP/ZnSe/ZnS quantum dot light-emitting diodes. *Nature* **2019**, *575*, 634–638. [[CrossRef](#)] [[PubMed](#)]
114. Alexandrov, A.; Zvaigzne, M.; Lypenko, D.; Nabiev, I.; Samokhvalov, P. Al-, Ga-, Mg-, or Li-doped zinc oxide nanoparticles as electron transport layers for quantum dot light-emitting diodes. *Sci. Rep.* **2020**, *10*, 7496. [[CrossRef](#)] [[PubMed](#)]
115. Moon, H.; Lee, W.; Kim, J.; Lee, D.; Cha, S.; Shin, S.; Chae, H. Composition-tailored ZnMgO nanoparticles for electron transport layers of highly efficient and bright InP-based quantum dot light emitting diodes. *Chem. Commun.* **2019**, *55*, 13299–13302. [[CrossRef](#)]
116. Dai, X.; Zhang, Z.; Jin, Y.; Niu, Y.; Cao, H.; Liang, X.; Chen, L.; Wang, J.; Peng, X. Solution-processed, high-performance light-emitting diodes based on quantum dots. *Nature* **2014**, *515*, 96–99. [[CrossRef](#)]
117. Lin, Q.; Wang, L.; Li, Z.; Shen, H.; Guo, L.; Kuang, Y.; Wang, H.; Li, L.S. Nonblinking quantum-dot-based blue light-emitting diodes with high efficiency and a balanced charge-injection process. *ACS Photonics* **2018**, *5*, 939–946. [[CrossRef](#)]
118. Kim, D.; Fu, Y.; Kim, S.; Lee, W.; Lee, K.H.; Chung, H.K.; Lee, H.J.; Yang, H.; Chae, H. Polyethylenimine ethoxylated-mediated all-solution-processed high-performance flexible inverted quantum dot-light-emitting device. *ACS Nano* **2017**, *11*, 1982–1990. [[CrossRef](#)]
119. Lee, T.; Hahm, D.; Kim, K.; Bae, W.K.; Lee, C.; Kwak, J. Highly efficient and bright inverted top-emitting InP quantum dot light-emitting diodes introducing a hole-suppressing interlayer. *Small* **2019**, *15*, 1905162. [[CrossRef](#)]
120. Li, D.; Bai, J.; Zhang, T.; Chang, C.; Jin, X.; Huang, Z.; Xu, B.; Li, Q. Blue quantum dot light-emitting diodes with high luminance by improving the charge transfer balance. *Chem. Commun.* **2019**, *55*, 3501–3504. [[CrossRef](#)]
121. Rhee, S.; Chang, J.H.; Hahm, D.; Jeong, B.G.; Kim, J.; Lee, H.; Lim, J.; Hwang, E.; Kwak, J.; Bae, W.K. Tailoring the electronic landscape of quantum dot light-emitting diodes for high brightness and stable operation. *ACS Nano* **2020**, *14*, 17496–17504. [[CrossRef](#)] [[PubMed](#)]
122. Moon, H.; Chae, H. Efficiency enhancement of all-solution-processed inverted-structure green quantum dot light-emitting diodes via partial ligand exchange with thiophenol derivatives having negative dipole moment. *Adv. Opt. Mater.* **2020**, *8*, 1901314. [[CrossRef](#)]
123. Lee, T.; Kim, B.J.; Lee, H.; Hahm, D.; Bae, W.K.; Lim, J.; Kwak, J. Bright and Stable Quantum Dot Light-Emitting Diodes. *Adv. Mater.* **2022**, *34*, 2106276. [[CrossRef](#)] [[PubMed](#)]

124. Rhee, S.; Hahm, D.; Seok, H.-J.; Chang, J.H.; Jung, D.; Park, M.; Hwang, E.; Lee, D.C.; Park, Y.-S.; Kim, H.-K. Steering Interface Dipoles for Bright and Efficient All-Inorganic Quantum Dot Based Light-Emitting Diodes. *ACS Nano* **2021**, *15*, 20332–20340. [[CrossRef](#)]
125. Kang, B.-H.; Lee, J.-S.; Lee, S.-W.; Kim, S.-W.; Lee, J.-W.; Gopalan, S.-A.; Park, J.-S.; Kwon, D.-H.; Bae, J.-H.; Kim, H.-R. Efficient exciton generation in atomic passivated CdSe/ZnS quantum dots light-emitting devices. *Sci. Rep.* **2016**, *6*, 34659. [[CrossRef](#)]
126. Bae, W.K.; Lim, J.; Zorn, M.; Kwak, J.; Park, Y.-S.; Lee, D.; Lee, S.; Char, K.; Zentel, R.; Lee, C. Reduced efficiency roll-off in light-emitting diodes enabled by quantum dot-conducting polymer nanohybrids. *J. Mater. Chem. C* **2014**, *2*, 4974–4979. [[CrossRef](#)]
127. Park, Y.; Klöckner, B.; Hahm, D.; Kim, J.; Lee, T.; Kim, J.; Bae, W.K.; Zentel, R.; Kwak, J. Origin of enhanced efficiency and stability in diblock copolymer-grafted Cd-free quantum dot-based light-emitting diodes. *J. Mater. Chem. C* **2021**, *9*, 10398–10405. [[CrossRef](#)]
128. Kim, L.A.; Anikeeva, P.O.; Coe-Sullivan, S.A.; Steckel, J.S.; Bawendi, M.G.; Bulović, V. Contact Printing of Quantum Dot Light-Emitting Devices. *Nano Lett.* **2008**, *8*, 4513–4517. [[CrossRef](#)]
129. Cho, H.; Kwak, J.; Lim, J.; Park, M.; Lee, D.; Bae, W.K.; Kim, Y.S.; Char, K.; Lee, S.; Lee, C. Soft Contact Transplanted Nanocrystal Quantum Dots for Light-Emitting Diodes: Effect of Surface Energy on Device Performance. *ACS Appl. Mater. Interfaces* **2015**, *7*, 10828–10833. [[CrossRef](#)]
130. Roh, H.; Ko, D.; Shin, D.Y.; Chang, J.H.; Hahm, D.; Bae, W.K.; Lee, C.; Kim, J.Y.; Kwak, J. Enhanced Performance of Pixelated Quantum Dot Light-Emitting Diodes by Inkjet Printing of Quantum Dot-Polymer Composites. *Adv. Opt. Mater.* **2021**, *9*, 2002129. [[CrossRef](#)]
131. Yang, J.; Hahm, D.; Kim, K.; Rhee, S.; Lee, M.; Kim, S.; Chang, J.H.; Park, H.W.; Lim, J.; Lee, M.; et al. High-Resolution Patterning of Colloidal Quantum Dots via Non-Destructive, Light-Driven Ligand Crosslinking. *Nat. Commun.* **2020**, *11*, 2874. [[CrossRef](#)] [[PubMed](#)]
132. Wood, V.; Panzer, M.J.; Chen, J.; Bradley, M.S.; Halpert, J.E.; Bawendi, M.C.; Bulović, V. Inkjet-Printed Quantum Dot-Polymer Composites for Full-Color AC-Driven Displays. *Adv. Mater.* **2009**, *21*, 2151–2155. [[CrossRef](#)]
133. Haverinen, H.M.; Myllylä, R.A.; Jabbour, G.E. Inkjet Printing of Light Emitting Quantum Dots. *Appl. Phys. Lett.* **2009**, *94*, 073108. [[CrossRef](#)]
134. Haverinen, H.M.; Myllylä, R.A.; Jabbour, G.E.; Cheng, M. Inkjet Printed RGB Quantum Dot-Hybrid LED. *J. Disp. Technol.* **2010**, *6*, 87–89. [[CrossRef](#)]
135. Still, T.; Yunker, P.J.; Yodh, A.G. Surfactant-Induced Marangoni Eddies Alter the Coffee-Rings of Evaporating Colloidal Drops. *Langmuir* **2012**, *28*, 4984–4988. [[CrossRef](#)] [[PubMed](#)]
136. Jiang, C.; Zhong, Z.; Liu, B.; He, Z.; Zou, J.; Wang, L.; Wang, J.; Peng, J.; Cao, Y. Coffee-Ring-Free Quantum Dot Thin Film Using Inkjet Printing from a Mixed-Solvent System on Modified ZnO Transport Layer for Light-Emitting Devices. *ACS Appl. Mater. Interfaces* **2016**, *8*, 26162–26168. [[CrossRef](#)] [[PubMed](#)]
137. Wang, J.; Dong, T.; Zhong, Z.; Zheng, H.; Xu, W.; Ying, L.; Wang, J.; Peng, J.; Cao, Y. Uniform Inkjet-Printed Films with Single Solvent. *Thin Solid Films* **2018**, *667*, 21–27. [[CrossRef](#)]
138. Yu, X.; Xing, R.; Peng, Z.; Lin, Y.; Du, Z.; Ding, J.; Wang, L.; Han, Y. To Inhibit Coffee Ring Effect in Inkjet Printing of Light-Emitting Polymer Films by Decreasing Capillary Force. *Chin. Chem. Lett.* **2019**, *30*, 135–138. [[CrossRef](#)]
139. Li, H.; Duan, Y.; Shao, Z.; Zhang, G.; Li, H.; Huang, Y.; Yin, Z. QLEDs: High-Resolution Pixelated Light Emitting Diodes Based on Electrohydrodynamic Printing and Coffee-Ring-Free Quantum Dot Film. *Adv. Mater. Technol.* **2020**, *5*, 2000401. [[CrossRef](#)]
140. Xiang, C.; Wu, L.; Lu, Z.; Li, M.; Wen, Y.; Yang, Y.; Liu, W.; Zhang, T.; Cao, W.; Tsang, S.W.; et al. High Efficiency and Stability of Ink-Jet Printed Quantum Dot Light Emitting Diodes. *Nat. Commun.* **2020**, *11*, 1646. [[CrossRef](#)]
141. Xie, L.; Yang, J.; Zhao, W.; Yi, Y.Q.Q.; Liu, Y.; Su, W.; Li, Q.; Lei, W.; Cui, Z. High-Performance Inkjet-Printed Blue QLED Enabled by Crosslinked and Intertwined Hole Transport Layer. *Adv. Opt. Mater.* **2022**, *10*, 2200935. [[CrossRef](#)]
142. Mei, W.; Zhang, Z.; Zhang, A.; Li, D.; Zhang, X.; Wang, H.; Chen, Z.; Li, Y.; Li, X.; Xu, X. High-Resolution, Full-Color Quantum Dot Light-Emitting Diode Display Fabricated via Photolithography Approach. *Nano Res.* **2020**, *13*, 2485–2491. [[CrossRef](#)]
143. Myeong, S.; Chon, B.; Kumar, S.; Son, H.J.; Kang, S.O.; Seo, S. Quantum Dot Photolithography Using a Quantum Dot Photoresist Composed of an Organic-Inorganic Hybrid Coating Layer. *Nanoscale Adv.* **2022**, *4*, 1080–1087. [[CrossRef](#)] [[PubMed](#)]
144. Wang, Y.; Fedin, I.; Zhang, H.; Talapin, D.V. Direct Optical Lithography of Functional Inorganic Nanomaterials. *Science* **2017**, *357*, 385–388. [[CrossRef](#)] [[PubMed](#)]
145. Wang, Y.; Pan, J.A.; Wu, H.; Talapin, D.V. Direct Wavelength-Selective Optical and Electron-Beam Lithography of Functional Inorganic Nanomaterials. *ACS Nano* **2019**, *13*, 13917–13931. [[CrossRef](#)]
146. Cho, H.; Pan, J.A.; Wu, H.; Lan, X.; Coropceanu, I.; Wang, Y.; Cho, W.; Hill, E.A.; Anderson, J.S.; Talapin, D.V. Direct Optical Patterning of Quantum Dot Light-Emitting Diodes via In Situ Ligand Exchange. *Adv. Mater.* **2020**, *32*, 2003805. [[CrossRef](#)]
147. Park, J.S.; Kyhm, J.; Kim, H.H.; Jeong, S.; Kang, J.; Lee, S.E.; Lee, K.T.; Park, K.; Barange, N.; Han, J.; et al. Alternative Patterning Process for Realization of Large-Area, Full-Color, Active Quantum Dot Display. *Nano Lett.* **2016**, *16*, 6946–6953. [[CrossRef](#)]
148. Hahm, D.; Lim, J.; Kim, H.; Shin, J.W.; Hwang, S.; Rhee, S.; Chang, J.H.; Yang, J.; Lim, C.H.; Jo, H.; et al. Direct Patterning of Colloidal Quantum Dots with Adaptable Dual-Ligand Surface. *Nat. Nanotechnol.* **2022**, *17*, 952–958. [[CrossRef](#)]
149. Kong, Y.L.; Tamargo, I.A.; Kim, H.; Johnson, B.N.; Gupta, M.K.; Koh, T.W.; Chin, H.A.; Steingart, D.A.; Rand, B.P.; McAlpine, M.C. 3D Printed Quantum Dot Light-Emitting Diodes. *Nano Lett.* **2014**, *14*, 7017–7023. [[CrossRef](#)]

150. Bae, J.; Lee, S.; Ahn, J.; Kim, J.H.; Wajahat, M.; Chang, W.S.; Yoon, S.Y.; Kim, J.T.; Seol, S.K.; Pyo, J. 3D-Printed Quantum Dot Nanopixels. *ACS Nano* **2020**, *14*, 10993–11001. [[CrossRef](#)]
151. Kim, B.H.; Onses, M.S.; Lim, J.B.; Nam, S.; Oh, N.; Kim, H.; Yu, K.J.; Lee, J.W.; Kim, J.H.; Kang, S.K.; et al. High-Resolution Patterns of Quantum Dots Formed by Electrohydrodynamic Jet Printing for Light-Emitting Diodes. *Nano Lett.* **2015**, *15*, 969–973. [[CrossRef](#)] [[PubMed](#)]
152. Guo, Y.; Moffitt, M.G. “Smart” Self-Assembled Quantum Dots Regulate and Stabilize Structure in Phase-Separated Polymer Blends. *Chem. Mater.* **2007**, *19*, 6581–6587. [[CrossRef](#)]
153. Zhao, J.; Chen, L.; Li, D.; Shi, Z.; Liu, P.; Yao, Z.; Yang, H.; Zou, T.; Zhao, B.; Zhang, X.; et al. Large-Area Patterning of Full-Color Quantum Dot Arrays beyond 1000 Pixels per Inch by Selective Electrophoretic Deposition. *Nat. Commun.* **2021**, *12*, 4603. [[CrossRef](#)] [[PubMed](#)]
154. Kang, H.L.; Kang, J.; Won, J.K.; Jung, S.M.; Kim, J.; Park, C.H.; Ju, B.K.; Kim, M.G.; Park, S.K. Spatial Light Patterning of Full Color Quantum Dot Displays Enabled by Locally Controlled Surface Tailoring. *Adv. Opt. Mater.* **2018**, *6*, 1701335. [[CrossRef](#)]